DOCUMENTATION OF THE MOVEMENT
OF THE HINTERES LANGTALKAR ROCK GLACIER

V. Kaufmann *, R. Ladstädter

Institute of Remote Sensing and Photogrammetry
Graz University of Technology, Austria
viktor.kaufmann@tugraz.at

KEY WORDS: Environment, Geomorphology, Change Detection, Monitoring, Aerial, Multitemporal, Digital, Photogrammetry

ABSTRACT:

Rock glaciers are striking phenomena of high mountain permafrost. These periglacial landforms are composed of rock and ice and creep downslope at a typical rate of a few decimeters per year. This movement and other surface changes can be measured by various observation techniques. In this paper a digital-photogrammetric approach to rock glacier monitoring is described based on multi-temporal aerial photographs. A software package, ADVM (Automatic Displacement Vector Measurement), has been developed, which automatically derives 3D displacement vectors from the photographs. The basic concepts of this software will be given first, followed by a detailed description of a new constrained image matching technique, implemented in the current ADVM 2.0 version. Finally, the successful application of the software is shown in a case study: The spatio-temporal evolution and dynamic behavior of the Hinteres Langtalkar rock glacier (Hohe Tauern range of the Austrian Alps) was reconstructed using aerial photographs (1954-1999). Results of the practical investigations are presented graphically and numerically.

1. INTRODUCTION

Rock glaciers are complex landforms of cold mountain areas and are composed of a mixture of rocks and ice. These unique features of mountain permafrost creep downslope by force of gravity in a steady-state mode due to the mainly plastic deformation of the interstitial ice, thus forming a characteristic surface topography consisting of transverse furrows and ridges (Barsch, 1996; Haeberli 2000). Rock glaciers play a decisive role in permafrost research, since recent climatic warming has triggered permafrost degradation. This fact may cause natural hazards, which are already observable in high-mountain areas, e.g. in the European Alps. The rock glacier system must be understood very well in order to correctly correlate observables of rock glaciers, e.g., creep velocity, temperature and ice content of the inner core, with climatic parameters, e.g., mean annual air temperature (Harris et al., 2001).

Contemporary rock glacier research is highly interdisciplinary. One special issue is to better understand rock glacier mechanics (Arenson et al., 2002; Ladanyi, 2003). Detailed knowledge of rock glacier kinematics is indispensable in this context. The creep process and also basal sliding at distinct shear horizons cause deformation of the permafrost body. Measurements of internal deformation, e.g., using inclinometers and magnet rings, can only be carried out in boreholes, which are expensive to drill and therefore limited to a few examples worldwide. In contrast, however, visible deformation of the rock glacier surface may be observed directly.

Monitoring of the temporal change of the surface geometry has already a long history. Kääb et al. (2003) give an overview of the state-of-the-art of the various monitoring techniques. Remote sensing, i.e., obtaining information without direct contact with the object, has been identified as one of the most powerful techniques. Referring to this technique, the development of digital photogrammetric procedures using aerial photographs has made substantial progress, and several applied studies have been published (Kääb et al., 2003; Kaufmann & Ladstädter, 2002; Kaufmann & Ladstädter, 2003).

In this paper we want to introduce our in-house developed software package ADVM (Automatic Displacement Vector Measurement). After describing the basic concepts of ADVM some technical details will be explained. Consequently, the applicability of the software will be shown in a case study. Finally, the paper concludes with recommendations for further developments.

2. METHOD

The first version of the ADVM software was developed in 1999. Since then, it has been further developed and used successfully in several rock glacier monitoring projects. This paper, however, will not describe the digital work flow of ADVM as a whole but focuses on a new matching algorithm, which has been developed especially for such monitoring tasks. The new algorithm, implemented in the recent ADVM 2.0 version, allows for high precision, multi-temporal point transfer in (pseudo-)rectified stereo pairs and simultaneous 3D reconstruction of displacement/flow vectors.

2.1 Basic Concepts

In this Section some of the basic concepts of the ADVM software will be outlined. The pseudo-orthophoto concept, being the key issue, will be discussed first. Some basics of the multi-photo constrained matching (MPCM) algorithm will then be described in brief. Finally, the extension of MPCM for multi-temporal point transfer is proposed.

---

* Corresponding author

2.1.1 Pseudo-orthophotos

The rectification of a single aerial photograph yields an orthophoto, which can only be called "true" if the DTM used is correctly representing the terrain surface. On the other hand, a rough DTM, which is only approximating the surface, can be used for the rectification of each stereo partner. This gives a new set of images, which we call "pseudo-orthophotos" (POPs). These images contain small deviations ΔR from the "true" orthophoto caused by the erroneous heights of the rough DTM (see Fig. 1). However, they have the same overall scale and orientation, which is an important property for facilitating matching. In combination with the rough DTM, POPs still contain the same stereo information as the original photographs, which enables strict photogrammetric 3D reconstruction. Using POPs for automated digital point transfer (matching) instead of the original photo scans has several advantages:

- Perspective distortions are removed to a great extent.
- Area-based matching methods, e.g., cross-correlation and least-squares matching, show an increased accuracy and robustness because of the more favorable geometry of POPs.
- Only the area of interest, i.e., the rock glacier and its surroundings, is covered by the POPs, therefore less computer storage is needed.
- 3D perception of motion parallaxes in multi-temporal POPs is possible, giving a first impression of the rock glacier creep and other surface changes.
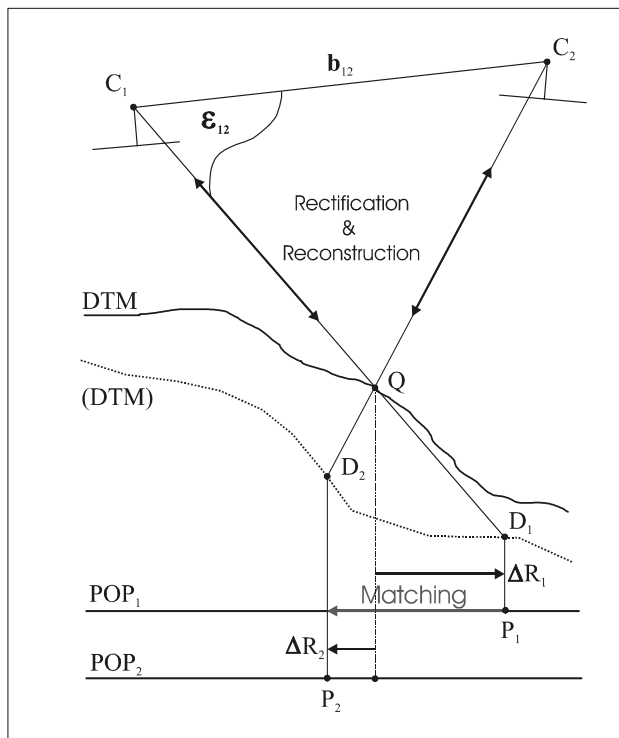
DTM   … true digital terrain model
(DTM)   … rough digital terrain model
ΔR_i … radial displacement in POP$_i$

Figure 1. Object point reconstruction with POPs

As mentioned before, a pair of POPs can be used for strict photogrammetric point reconstruction in object space. For the corresponding points P_1 and P_2 in the POPs, the height is interpolated in the rough DTM, which yields the intersection points D_1 and D_2, respectively. The projection rays passing through the projection center C_1 and C_2 coincide with the rays used in the rectification process and also allow for forward intersection of the object point Q. This concept has already been proposed for DTM generation (Schenk et al., 1990) and more generally outlined for the extraction of 3D information from rectified stereo pairs (Baltsavias, 1996).

It is important to note that deviations of the rough DTM from the true terrain surface do not introduce any systematic errors for the reconstructed object point position (however, increasing height deviations will cause additional perspective distortions resulting in reduced matching accuracy). If, on the other hand, a single orthophoto is used for the extraction of a 3D point position, the radial displacements of points not lying on the given DTM are not corrected for. Thus, POPs derived from a DTM of good quality should be used for digital point transfer if high photogrammetric precision is needed.

2.1.2 Constrained matching using the MPCM algorithm

Multi-photo (geometrically) constrained matching (MPCM) was introduced by Grün and Baltsavias (1988). This algorithm combines least-squares matching (LSM) in multiple images with simultaneous determination of the associated object point in a single, iterative adjustment process. The unknown object coordinates and the matched image positions found by LSM are connected via the collinearity equations. Fixing a selected (interest) point in the reference image forces the corresponding points in the other images to lie on their epipolar lines. This epipolar constraint reduces the search space from 2D to 1D, thus making the MPCM algorithm more robust and also more accurate than the free, unconstrained LSM. A detailed description and extensive investigation of the algorithm can be found in Baltsavias (1991).

Because of its robustness and high matching accuracy the MPCM algorithm is considered to be a perfect tool for photogrammetric rock glacier monitoring. It is implemented as a single module in the current version 2.0 of the ADVM software, replacing both the (unconstrained) LSM module and reconstruction module of the prior version. The standard MPCM algorithm had to be adapted (1) for multi-temporal matching and (2) for matching in POPs.

2.1.3 Multi-temporal point transfer in image sequences

In a rock glacier monitoring project stereo photographs of at least two epochs must be available. A prominent point (e.g. a boulder) on the rock glacier surface can be tracked in the image sequence as it moves due to rock glacier flow. MPCM can be used for this multi-temporal point transfer but must be extended for simultaneous determination of the object point in every epoch. This can be done by adding three additional object coordinate unknowns for each new epoch to the MPCM system.

For such a multi-temporal MPCM system, e.g., containing two epochs, the unknown object points Q_1 and Q_2 are part of the parameter vector. After the system is solved, the displacement

vector $\mathbf{f}_{12} = \mathbf{Q}_2 - \mathbf{Q}_1$ can be calculated, which corresponds to the rock glacier flow between these two epochs.

The combined system offers the possibility to introduce additional constraints between the object points Q_1 and Q_2. Constraints controlling direction and/or length of the flow vector can therefore be directly integrated into the matching process. One implementation of such a flow constraint is described in Section 2.2.3.

2.2 Modifications of the standard MPCM algorithm

In this Section the standard MPCM algorithm (using central perspective images) will be adapted for direct matching in POPs. First, the well-known collinearity equations are replaced by a modified function, which describes the projection of an arbitrary point Q in object space into a POP (next Section). Furthermore, a linearized form of this function will be derived, which allows geometric constraints to be formulated in the same way as in the standard MPCM (Section 2.2.2).

2.2.1 Modified collinearity equations

The projection ray p_i is defined by the projection center C_i and a given object point Q. Intersecting this ray with the rough DTM yields the intersection point D'_i. This point must be projected into the ground plane to obtain the corresponding point P'_i in the image POP$_i$ (see Figure 2).

Instead of the strict, iterative DTM intersection a more coarse method will be used: At an approximate position (D_i) on the rough DTM the normal vector n_i is calculated, defining the tangential plane in this point. Intersecting the projection ray with this plane gives only an approximate solution, but has two advantages:

- Direct and fast computation of the intersection point.
- The projection of an object point into a POP can be given in closed formulas.

Using this method, the calculation of the intersection point is straightforward:

$$\mathbf{D}'_i = \mathbf{C}_i + \lambda_i \cdot \mathbf{p}_i \quad with \quad \lambda_i = \frac{((\mathbf{D}_i) - \mathbf{C}_i) \cdot \mathbf{n}_i}{\mathbf{p}_i \cdot \mathbf{n}_i} \qquad (1)$$

where $\mathbf{p}_i = \mathbf{Q} - \mathbf{C}_i \ldots$ projection ray.

The origin of the image coordinate system of the POP is located at position X_0^{POP} in the object coordinate system (x-axis parallel to the X-axis, y-axis opposite to the Y-axis, pixel size ΔX and ΔY). Then Equation (2) can be used to transform the planimetric X- and Y-coordinates of $\boldsymbol{D}'_i$ into the image coordinates x'_p, y'_p of the projected point P'_i:

$$x'_{p_i} = \left(D'^X_i - X_0^{POP}\right) / \Delta X = G_i^x$$
$$y'_{p_i} = -\left(D'^Y_i - Y_0^{POP}\right) / \Delta Y = G_i^y \qquad (2)$$

Equation (2) permits the computing of the projected point in the POP associated with C_i from a given object point Q. This function thus represents the modified collinearity equation and will be called G_i^x and G_i^y, respectively, for the x- and y-component of the projected point.

In the MPCM adjustment the linearized form of (2) is needed, which relates small changes in the object point coordinates to a translation of the projected point in the POP:

$$dx'_{p_i} = \frac{\partial G_i^x}{\partial X} \cdot dX + \frac{\partial G_i^x}{\partial Y} \cdot dY + \frac{\partial G_i^x}{\partial Z} \cdot dZ$$
$$dy'_{p_i} = \frac{\partial G_i^y}{\partial X} \cdot dX + \frac{\partial G_i^y}{\partial Y} \cdot dY + \frac{\partial G_i^y}{\partial Z} \cdot dZ \qquad (3)$$

In order to derive the partial derivatives of functions G_i^x and G_i^y, a linearization of Equation (1) with respect to the object point Q has to be done:

$$d\mathbf{D}'_i = d\lambda_i \cdot \mathbf{p}_i + \lambda_i \cdot d\mathbf{p}_i = \lambda_i \cdot \left(d\mathbf{p}_i - \frac{(\mathbf{n}_i \cdot d\mathbf{p}_i)}{(\mathbf{n}_i \cdot \mathbf{p}_i)} \cdot \mathbf{p}_i \right) \quad (4)$$

where $d\mathbf{p}_i = d\mathbf{Q} = \begin{pmatrix} dX \\ dY \\ dZ \end{pmatrix}$ … translation of the object point.

From Equation (4) the first and second component D'^X_i and D'^Y_i can be extracted and inserted into the linearized form of Equation (2). Replacing the term $d\mathbf{p}_i$ by $d\mathbf{Q}$ and sorting for parameters dX, dY and dZ, respectively, gives the partial derivatives of the modified collinearity equations, listed explicitly in Equation (5):

$$\frac{\partial G_i^x}{\partial X} = \frac{\lambda_i}{\Delta X} \left(1 - \frac{n_i^X \cdot p_i^X}{(\mathbf{n}_i \cdot \mathbf{p}_i)} \right), \quad \frac{\partial G_i^x}{\partial Y} = \frac{\lambda_i}{\Delta X} \left(- \frac{n_i^Y \cdot p_i^X}{(\mathbf{n}_i \cdot \mathbf{p}_i)} \right);$$

$$\frac{\partial G_i^x}{\partial Z} = \frac{\lambda_i}{\Delta X} \left(- \frac{n_i^Z \cdot p_i^X}{(\mathbf{n}_i \cdot \mathbf{p}_i)} \right), \quad \frac{\partial G_i^y}{\partial X} = \frac{\lambda_i}{\Delta Y} \left(\frac{n_i^X \cdot p_i^Y}{(\mathbf{n}_i \cdot \mathbf{p}_i)} \right); \quad (5)$$

$$\frac{\partial G_i^y}{\partial Y} = \frac{\lambda_i}{\Delta Y} \left(\frac{n_i^Y \cdot p_i^Y}{(\mathbf{n}_i \cdot \mathbf{p}_i)} - 1 \right), \quad \frac{\partial G_i^y}{\partial Z} = \frac{\lambda_i}{\Delta Y} \left(\frac{n_i^Z \cdot p_i^Y}{(\mathbf{n}_i \cdot \mathbf{p}_i)} \right).$$

2.2.2 Epipolar constraint for POPs

Epipolar geometry can also be used to constrain matching in POPs. The situation with POPs is more complex, however, because of the DTM involved. In general, the epipolar line in the POP will no longer be a straight line but a general curve. This can be seen by intersecting the epipolar plane with the rough DTM. The projection of this intersection curve into the ground plane yields an "epipolar curve" in the POP. The tangent line at a certain point on this curve therefore corresponds to the epipolar line of a perspective image.
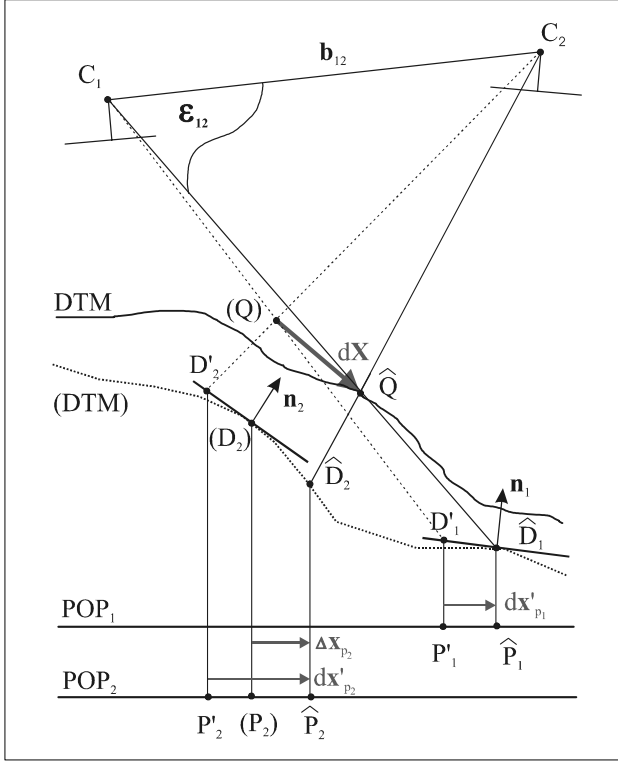
Figure 2. Constrained matching in POPs

Constrained matching in POPs will be described in detail in the following. Figure 2 depicts the situation for a pair of POPs, with POP_1 being the reference image. The object point is shown in its initial position (Q). During the iterative adjustment procedure, the object point is shifted by the vector dX, until its final position $\hat{Q}$ on the true DTM is found (intermediate positions are not shown here). Least-squares matching is performed in the POPs, with the template centered on the fixed point $\hat{P}_1$ in the reference image. The matching window is moving in POP_2, centered on the approximate position (P_2). In each iteration step, the object point is projected into the POPs using the intersection method described in Section 2.2.1. As long as no consistent solution is found, the projected points P'_1 and P'_2 will not coincide with the matched positions $\hat{P}_1$ and (P_2). To achieve this, the following geometric constraints must be added to the MPCM system for each image:

$$(x_{p_i}) + \Delta x_{p_i} \overset{!}{=} x'_{p_i} + dx'_{p_i}$$
$$(y_{p_i}) + \Delta y_{p_i} \overset{!}{=} y'_{p_i} + dy'_{p_i}$$

(6)

where: (x_{p_i}) ... approximated position in the POP image

Δx_{p_i} ... LSM translation parameter

x'_{p_i} ... projected object point in the POP

dx'_{p_i} ... shift of the projected point due to an object point shift (see Equation (3)).

For the reference image the LSM shift parameters are set to zero, which forces the object point to lie on the projection ray defined by $\hat{D}_1$. As the tangential plane is fixed at this point, the geometric constraint is strict and the projected point will

already coincide after the first iteration. The fixed ray and the basis vector b_{12} define the epipolar plane ε_{12}.
In the second image, the point (P_2) is shifted by the LSM process. The normal vector n_2 defining the tangential plane must therefore be recalculated in each iteration. As (D_2) converges towards $\hat{D}_2$, the intersection becomes more and more accurate. Thus, the solution for D'_2 will be strict in the final position. The intersection line of the tangential plane with the epipolar plane ε_{12} defines the epipolar line in object space. Applying the geometric constraint (6) to the second image forces the matched point to lie on the tangent line of the epipolar curve at point $\hat{P}_2$.

As described above, the implementation of the epipolar constraint is done by adding geometric constraints for each image to the MPCM system. Inserting Equation (3) into (6) gives the modified geometric constraint for POPs. The constraints are introduced to the MPCM system as pseudo-observations with a certain weight as follows:

$$(x_{p_i}) - x'_{p_i} + v_i^x = \frac{\partial G_i^x}{\partial X} dX + \frac{\partial G_i^x}{\partial Y} dY + \frac{\partial G_i^x}{\partial X} dZ - \Delta x_{p_i} \quad (7)$$
$$(y_{p_i}) - y'_{p_i} + v_i^y = \frac{\partial G_i^y}{\partial X} dX + \frac{\partial G_i^y}{\partial Y} dY + \frac{\partial G_i^y}{\partial X} dZ - \Delta y_{p_i}$$

2.2.3 Introducing the flow constraint

As already mentioned in Section 2.1.3, additional constraints applied to the object coordinates can be introduced in a multi-temporal MPCM system. This means, that the flow vector $\mathbf{f}_{rs} = \mathbf{Q}_s - \mathbf{Q}_r$ can be constrained to a certain direction/length obtained from a specific flow model.

As rock glacier flow is known to be driven mainly by gravity, the displacement will follow more or less the gradient direction of the DTM. In the reference epoch the gradient g_r of the rough DTM is calculated at position Q_r. For a second epoch, the flow constraint $\mathbf{f}_{rs} \cdot \mathbf{g}_r^{\perp} = 0$ can be formulated.

Because the Z-component is considered to be less accurate, the flow constraint will only be applied to the X- and Y-components of the flow vector. After linearization with respect to the object point coordinates the flow constraint can be introduced to the MPCM system as a pseudo-observation:

$$\mathbf{f}_{rs} \cdot \mathbf{g}_r^{\perp} + v_r = -(dX_s - dX_r) \cdot g_r^Y + (dY_s - dY_r) \cdot g_r^X \quad (8)$$

Depending on the weight selected, the flow constraint will be more or less strict, which must be controlled by the user. If the weight chosen is too high, matching will fail, because of errors contained in the flow model. Applied with a suitable weight, however, the flow constraint will automatically exclude false matches from the measured flow vector field.

In this Chapter a detailed description of the new matching algorithm implemented in the ADVM 2.0 software has been provided. The following Chapter will present a case study of a rock glacier monitoring project performed with ADVM.

3. CASE STUDY

The Hinteres Langtalkar rock glacier (12°45'56" E, 46°58'53" N) is located in the Schober group of the Hohe Tauern range within the boundaries of the Austrian Hohe Tauern National Park (see Fig. 3). The rock glacier is situated in the Hinteres Langtal cirque (see Fig. 4). The foot of the front slope is located at 2460 m a.s.l. The northern lobe of the rock glacier is 850 m long and 200 m wide. This highly active part of the rock glacier is in contrast to the rather inactive southern, smaller part of the rock glacier. The latter is characterized by a sequence of adjacent ridges and furrows, which typically relates to compressive flow. At the rooting zone of both parts of the rock glacier marked depressions are present. Further information about the geographical setting and results of geological and hydrological investigations can be found in Lieb (1987) and Krainer & Mostler (2001), respectively.
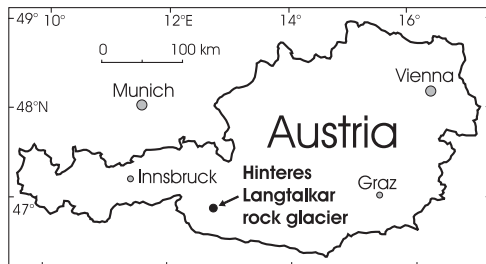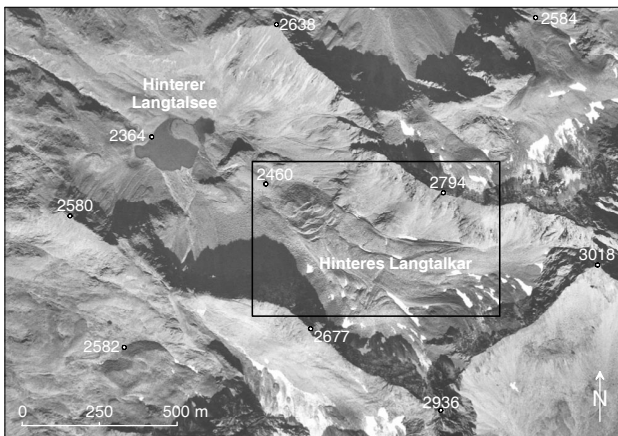

Figure 3. Location map of the study area

Figure 4. Orthophoto (9.9.1997) of the study area showing the Hinteres Langtalkar rock glacier. The box delineates the area shown in Figures 5-7.

The Hinteres Langtalkar rock glacier is very interesting from a geomorphological point of view, since the lower end of the rock glacier tongue has moved into steeper terrain. A sliding process has started as early as 1992, as the strength of the ice/rock mixture could no longer resist gravitational forces. This phenomenon was identified for the first time in aerial photographs of 1997 (cp. Fig. 4). A similar geomorphological situation is known from the Äusseres Hochebenkar rock glacier, Austria (see Kaufmann & Ladstädter, 2003). A monitoring program has been initiated in order to study the morphodynamics of the Hinteres Langtalkar rock glacier in more detail. The program includes (1) reconstruction of the past kinematic state of the rock glacier using aerial photographs, (2) determination of the present movement by means of geodetic survey, and (3) investigation of alternative monitoring

techniques, such as terrestrial laser scanning and satellite-based radar interferometry. Some results of the photogrammetric work are presented in the following Section. Geodetic work is briefly outlined in Kaufmann & Ladstädter (2003). Concerning the alternative monitoring techniques the reader is referred to Bauer et al. (2003) and Kenyi & Kaufmann (2003).

3.1 Results of digital photogrammetric work

Aerial photographs at various scales of 11 different overflights between 1954 and 1999 were made available for detailed photogrammetric analysis in order to study the spatio-temporal evolution and kinematic behavior of the rock glacier. The main task was to derive 3D displacement/flow vectors using ADVM software. In a first step all photographs, except those of 1954 which show a thin snow cover, were photogrammetrically orientated using a Kern DSR-1 analytical plotter. A digital photogrammetric workstation of Z/I Imaging was at our disposal later. Subsequently, all photographs were digitized with a resolution of 10 µm using an UltraScan 5000 of Vexcel Imaging Austria. Elements of exterior orientation were taken from the analytical plotter. The stereopair of 1998 was selected for detailed photogrammetric mapping of the rock glacier and its surroundings. This work was done manually at the analytical plotter in order to achieve high accuracy and geomorphic acuity. A similar procedure was performed for the stereopair of 1974. However, the mapping was limited to the area covered by the rock glacier. High resolution digital terrain models with a grid spacing of 2 m were derived from both data sets. Pseudo-orthophotos with a pixel size of 0.25 m were computed from all photographs selected. Photographs of 1992 and older were (pseudo-)rectified using the DTM of 1974, the younger ones using the DTM of 1998. All pseudo-orthophotos were processed with ADVM software. Finally, 3D displacement vectors were obtained. In this paper we present a graphical representation of the spatial distribution of the horizontal creep velocity for the time period 1969-1974 (cp. Figs. 5-7).

We can summarize the main findings of the case study as follows: The creeping process of the rock glacier has remained steady over the years with flow/creep velocities increasing from the root towards the lower end (frontal slope). A mean annual horizontal flow velocity for the time period 1969-1991 was measured at 1.35 m/year at the upper rim of the frontal slope. A landslide occurred at the steep frontal slope of the rock glacier between 1992 and 1997. The photogrammetric measurements of three observation periods after 1997 reveal that the flow velocity has significantly increased at the lower part of the rock glacier (max. horizontal movement of up to 2.8 m/year) compared to previous years. Distinct crevasses with high longitudinal strain rates have developed as a result of the extending flow/creep process. Photogrammetric results were checked by means of precise annual geodetic measurements (1999-2003).

4. CONCLUSIONS

With the present case study we could demonstrate that the proposed digital photogrammetric method of deformation measurement from multi-temporal aerial photographs is feasible and that the movement of the rock glacier could be measured with high accuracy. Further developments of ADVM software will address robust matching in difficult areas, i.e., with low or missing texture, snow patches and cast shadows. Additional applied studies must be carried out in order to better tune the various parameters needed in the semi-automatic workflow.
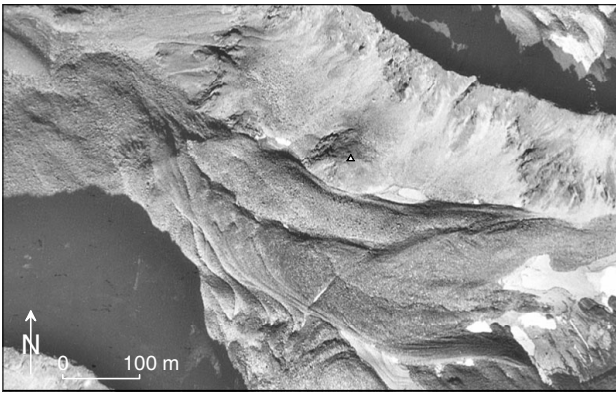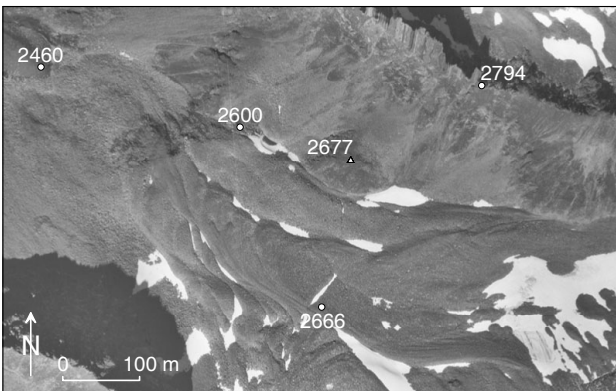
Figure 5. Hinteres Langtalkar rock glacier (9.10.1969)
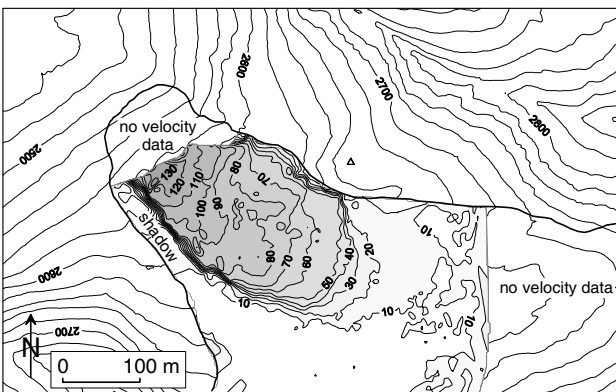

Figure 6. Hinteres Langtalkar rock glacier (5.9.1974)

Figure 7. Mean annual horizontal creep velocity (cm a^{-1}) at the Hinteres Langtalkar rock glacier for the time period 1969-1974.

REFERENCES

Arenson, L., Hoelze, M., Springman, S., 2002. Borehole Deformation Measurements and Internal Structure of Some Rock Glaciers in Switzerland. *Permafrost and Periglacial Processes*, 13(2), pp. 117-135.

Baltsavias, E.P., 1991. Multiphoto Geometrically Constrained Matching. *Mitteilungen des Instituts für Geodäsie und Photogrammetrie*, ETH Zürich, 49, 221 p.

Baltsavias, E.P., 1996. Digital ortho-images − a powerful tool for the extraction of spatial and geo-information. *ISPRS Journal of Photogrammetry and Remote Sensing*, 51, pp. 63-67.

Barsch, D., 1996. Rockglaciers: Indicators for the Present and Former Geoecology in High Mountain Environments. *Springer Series in Physical Environment*, 331 p.

Bauer, A., Paar, G., Kaufmann, V., 2003. Terrestrial laser scanning for rock glacier monitoring. In: *Proceedings of the 8th Int. Conf. on Permafrost*, Zurich, Vol. 1, A.A. Balkema Publishers, pp. 55-60.

Grün, A. & Baltsavias, E.P., 1988. Geometrically constrained multiphoto matching. In: *PE&RS* (54) 5, pp. 633-641.

Haeberli, W., 2000. Modern Research Perspectives Relating to Permafrost Creep and Rock Glaciers: A Discussion. *Permafrost and Periglacial Processes*, 11(4), pp. 290-293.

Harris, C., Davies, M.C.R.; Etzelmüller, B., 2001. The Assessment of Potential Geotechnical Hazards Associated with Mountain Permafrost in a Warming Global Climate. *Permafrost and Periglacial Processes*, 12(1), pp. 145-156.

Kääb, A., Kaufmann, V., Ladstädter, R., Eiken, T., 2003. Rock glacier dynamics: implications from high-resolution measurements of surface velocity fields. In: *Proceedings of the 8th Int. Conf. on Permafrost*, Zurich, Vol. 1, A.A. Balkema Publishers, pp. 501-506.

Kaufmann, V. & Ladstädter, R., 2002. Monitoring of active rock glaciers by means of digital photogrammetry. In: *IAPRS*, Graz, Austria, XXXIV, Part 3B, Comm. III, pp. 108-111.

Kaufmann, V. & Ladstädter, R., 2003. Quantitative analysis of rock glacier creep by means of digital photogrammetry using multi-temporal aerial photographs: two case studies in the Austrian Alps. In: *Proc. of the 8th Int. Conf. on Permafrost*, Zurich, Vol. 1, A.A. Balkema Publishers, pp. 525-530.

Kenyi, L.W. & Kaufmann, V., 2003. Measuring rock glacier surface deformation using SAR interferometry. In: *Proceedings of the 8th Int. Conf. on Permafrost*, Zurich, Vol. 1, A.A. Balkema Publishers, pp. 537-541.

Krainer, K. & Mostler, W., 2001. Der aktive Blockgletscher im Hinteren Langtal Kar, Gößnitztal (Schobergruppe, Nationalpark Hohe Tauern). In: *Wissenschaftliche Mitteilungen aus dem Nationalpark Hohe Tauern*, Matrei, 6, pp. 139-168.

Ladanyi, B., 2003. Reology of ice/rock systems. In: *Proceedings of the 8th Int. Conf. on Permafrost*, Zurich, Vol. 1, A.A. Balkema Publishers, pp. 621-626.

Lieb, G.K., 1987. Die Gletscher und Blockgletscher im Kärntner Teil der Schobergruppe und ihre Entwicklung seit dem Spätglazial. *Unpubl. Dissertation*, Univ. of Graz, 286 p.

Schenk, T., Li, J.-C., Toth, C.K., 1990. Hierarchical approach to reconstruct surfaces by using iteratively rectified imagery. In: *Close-Range Photogrammetry Meets Machine Vision*, International Archives of Photogrammetry and Remote Sensing, 28 (5/1), SPIE 1395 (1), pp. 464-470.